

Received March 1, 2020, accepted March 17, 2020, date of publication March 25, 2020, date of current version April 15, 2020.

Digital Object Identifier 10.1109/ACCESS.2020.2983260

# Modeling and Experimental Study of a Novel Multi-DOF Parallel Soft Robot

JIE ZHANG<sup>1,2</sup>, HANG WEI<sup>3</sup>, YU SHAN<sup>3</sup>, PENGBO LI<sup>3</sup>, YANZHI ZHAO<sup>3</sup>, LIZHE QI<sup>4</sup>, AND HONGNIAN YU<sup>5</sup>

<sup>1</sup>Liren College, Yanshan University, Qinhuangdao 066004, China

<sup>2</sup>Institute of Electrical Engineering, Yanshan University, Qinhuangdao 066004, China

<sup>3</sup>Key Laboratory of Parallel Robots and Mechatronic Systems, Yanshan University, Qinhuangdao 066004, China

<sup>4</sup>Academy for Engineering and Technology, Fudan University, Shanghai 200433, China

<sup>5</sup>School of Engineering and Built Environment, Edinburgh Napier University, Edinburgh EH10 5DT, U.K.

Corresponding authors: Yanzhi Zhao (yzzhao@ysu.edu.cn), Lizhe Qi (qilizhe@fudan.edu.cn), and Hang Wei (weihang@stunmail.ysu.edu.cn)

This work was supported in part by the National Key Research and Development Program under Grant 2017YFE0112200, in part by the Natural Science Foundation of Hebei Province under Grant E2018203436, in part by the Science Technology Research of Higher Education of Hebei Province under Grant ZD2018024, in part by the Jihua Laboratory, Guangdong, under Grant Y80311W180, and in part by the Graduate innovation funding program of Hebei Province under Grant CXZZSS2020043.

**ABSTRACT** In view of the demand for flexible drive and large load of the soft robot in the practical application, a novel type of flexible-actuated multi-degree-of-freedom (multi-DOF) parallel soft robot is designed. The proposed robot in parallel combination of three groups of flexible-actuated elements (FAEs) realizes large load by increasing the bearing area at the connection between flexible-actuated units (FAUs). In order to improve the driving flexibility, the multi-layer FAU is used to drive independently in parallel so as to realize omnidirectional bending movement by pneumatic drive. With the coupled analysis in terms of motion and force, the mapping model of kinematic attitude parameters and the external load force with output air pressure value is established. Finally, an experimental prototype is developed and an experimental test platform is built. Then, the comparison among the experimental data, simulation results and theoretical results verifies the capability of multi-DOF omnidirectional movement and flexible-actuated large load.

**INDEX TERMS** Flexible drive, large load, kinematic and static models, parallel soft robot.

## I. INTRODUCTION

Due to the arbitrary change of shape and strong environment adaptability, the soft robot [1], [2] is capable of completing complex tasks with broad application prospects ranging from medical rehabilitation [3], search and inspection [4], [5] to rescue operation [6].

Usually made of flexible materials, the soft robot is characterized by high motion flexibility and completion of complex movements under simple drives. Currently, there are two main types of soft robots: one is to use flexible smart materials to generate movement through deformation under the action of external physical field. The other type is to use the soft material (e.g. silicon rubber) to realize the kinematic deformation by pneumatic drive.

In recent years, the first type of soft robots made of flexible smart materials developed rapidly. Cheng *et al.* [7] proposed

The associate editor coordinating the review of this manuscript and approving it for publication was Hui Xie <sup>1</sup>.

a type of shape memory alloy driven multi-DOF soft robot based on SMA material drive. Although SMA deforms under the control of external temperature with a high mass stress ratio, the stress produced by SMA is greatly affected by temperature. In addition, the efficiency is relatively low since most of the input energy is consumed during heating. Li [8], Mutlu *et al.* [9] designed a soft robot based on the electroactive polymer which changes the internal structure of the material to form deformation movement under the action of external electric field. However, the bearing capacity is relatively low due to the low intensity of the material.

Compared with the first type of soft robot, the second type is applied by many scholars at present because of its mature pneumatic driving technology, faster reaction speed, higher power density and lower cost. Zhang *et al.* [10] proposed an omnidirectional soft robot composed of pneumatic soft actuators. In order to maintain walking balance, three identical pneumatic flexible soft legs, made of cylindrical soft body with three identical cavities in the middle, are adopted which

resulted in low structural rigidity, reduced motion stability and low bearing capacity. In order to solve such problems as low load and poor structural stability, Rivera [11] and [14], and Hopkins *et al.* [13] proposed a new type of parallel soft robot based on TCAs. Made of silicone rubber, the driving unit consists of three cylindrical cavities, which can be bent and extended in accordance with the change of air pressure of three cavities. Moreover, the driving unit is combined to synthesize a soft robot with tetrahedral structure so as to enhance the structural rigidity and improve the bearing capacity. However, the kinematic deformation is difficult to control because of the complex driving structure. Moreover, the flexibility of kinematic deformation is reduced because of the cylindrical cavity structure of the driving unit which leads to the small range of axial extension movement. In order to enhance the ability to bend or stretch, Drotman [14] proposed a kind of soft pneumatic actuator similar to bellows structure, based on which a four-legged soft robot is designed. Due to good axial expansion deformability of the bellows structure, the four-legged soft robot has stronger kinematic deformability and better flexibility. However, in some high-intensity applications, the bellows structure is prone to fold or fail when subjected to a large load, resulting in a smaller load-carrying capacity. In order to improve carrying capacity by increasing resistance to distortion and a folding structure, this paper proposes a soft parallel structure based on the parallel mechanism to enhance the bearing capacity by increasing the bearing area at the connection of each layer of FAEs. Furthermore, FAEs are divided into multi-layer FAUs driven independently in parallel, so the multi-DOF omnidirectional bending motion is realized to increase the driving flexibility.

The modeling of continuous soft robot has been facing many challenges [1] because of the uncertain influence factors in motion and under load and the easily affected shape by the external load. Currently, there are two main modeling methods: one is based on the theory of Cosserat Rod, the other is based on robots with constant curvature, which is usually considered as the most common method of continuous robot modeling by the constant curvature approximation [15], [16]. Katzschmann *et al.* [17] analyzed the kinematics of the multiple segment soft robot based on the piecewise constant curvature. However, the low calculation efficiency of the model is not conducive to practical application because of the relatively complex model. Dehghani and Moosavian [18], [19] developed statics model mainly for non-stretching continuum robots, but it is not for the soft robot with continuous stretching deformability. Since the nonlinear response of soft robot materials complicates the calculation, some researchers proposed to divide the modeling process into two parts: (1) obtain the relationship between pressure and the length of the cavity by experimental fitting, (2) convert the length of cavity to the end coordinates of the soft arm [20], [21]. However, the analysis was carried out without taking gravity and load into consideration to reduce modeling complexity. Qi *et al.* [22] put forward a method for analyzing the flexibility of the planar spring and derived the flexibility

matrix to represent force-deflection relationship in order to achieve accurate motion prediction. However, the model fails to respond quickly in engineering applications because of the large amount of calculation requiring multiple integration operations. It is difficult to establish a complete mathematical model for a parallel-structured soft robot, so Zhang *et al.* [23] proposed a mathematical model with a phenomenological modeling method. The properties of ePSA are described by the phenomenological model, and the contraction force in the model is replaced by thrust. The ePSA is equivalent to a ternary model composed of thrust unit, spring unit and damping unit in parallel [24]. At the same time, the robot is regarded as a constant curvature arc, and a unified constant curvature kinematic model is established [25], [26]. Therefore, in this paper, a better modeling analysis on pneumatic parallel soft robot in various kinematic and force states is carried out to reduce the complexity and improve the efficiency of the model calculation. Firstly, the mapping model between the attitude parameters and the input air pressure without external load is established to determine the motion attitude of the parallel robot. Secondly, the single branch FAE of the parallel soft robot is simplified as an elastic model to build a force analysis model, which can analyze the force of the parallel soft robot under different load conditions. Finally, the mapping model between the deformation parameters and the external load with the input air pressure of the parallel soft robot is established. Hence, the coupling analysis of the deformation and the force of the parallel soft robot is carried out to realize the unified control of the movement and output force, which facilitates the control of the parallel soft robot.

The rest of the paper is organized as follows. In Section II, the structural characteristics of parallel soft robot are introduced, in Section III, the mapping model between the attitude parameters and the input air pressure of the parallel robot is derived. In Section IV, the attitude of the parallel soft robot is determined with the model established in the previous section, and the force analysis and static model of the parallel soft robot are established. In Section V, the finite element simulation is carried out. In Section VI, the prototype is tested, and the final conclusion is drawn in the seventh section.

## II. STRUCTURAL CHARACTERISTICS OF PARALLEL SOFT ROBOTS

### A. OVERALL STRUCTURAL CHARACTERISTICS OF ROBOTS

The advantages of the traditional parallel robots [27], such as large rigidity, stable and compact structure, strong bearing capacity and so on [28], has been integrated into the soft robot, hence, the parallel soft actuated structure is proposed. Based on this actuated structure, this paper proposes a novel type of multi-DOF parallel soft robot, which is composed of three identical groups of FAEs in parallel with a large bearing capacity under external load. Made of soft material and driven independently in parallel by multi-layer FAUs, the FAEs equip the parallel soft robot with multi-DOF

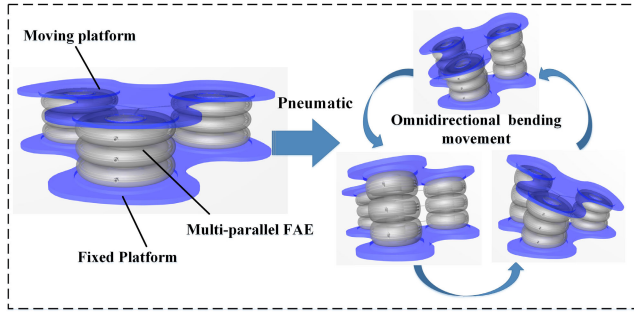


FIGURE 1. Multi-DOF parallel soft robot.

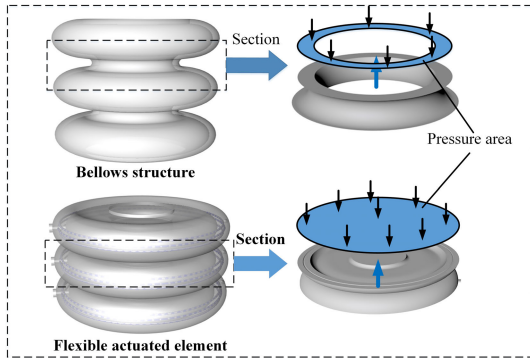


FIGURE 2. Forced area comparison.

motion ability. Therefore, the omnidirectional bending motion of the parallel soft robot can be realized by controlling the air pressure inside the actuated element, as shown in Fig. 1.

**B. STRUCTURAL CHARACTERISTICS OF FAE**

The FAE of the traditional soft robot mostly adopts the cylindrical bellows structure with radial corrugations with good bending ability, however, when it is subjected to external load, the force area between each layer is reduced because the two adjacent layers are connected by rings as shown in Fig. 2. Therefore, both the transmitted air pressure load force and the overall structural rigidity being reduced, the robot may result in torsional deformation when subjected to large pressure loads and bending moments, as shown in Fig. 3, with the ultimate result of reduced bearing capacity. The plane connection between the two adjacent layers of the FAE designed in this paper, as shown in Fig. 2, increases the connection area between the layers of the FAEs, thus increasing the force-bearing area when transferring the load and enhancing the overall structural rigidity of the FAE, resisting torsional deformation when subjected to the pressure load. Finally, the bearing capacity of the FAE in various states is improved, and then the bearing capacity of the parallel soft robot is enhanced.

In order to improve the flexibility of the FAE of the soft robot, this paper divides the FAE into three layers of independent structure, with each layer drive being independent and controllable to be capable of multi-DOF bending movement in order to improve the bending deformability of the FAE.

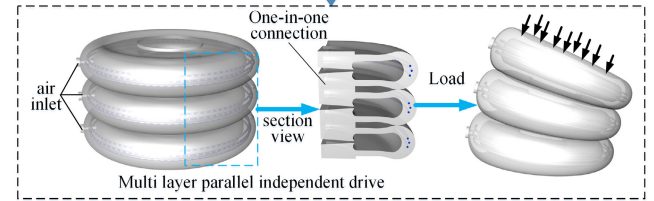
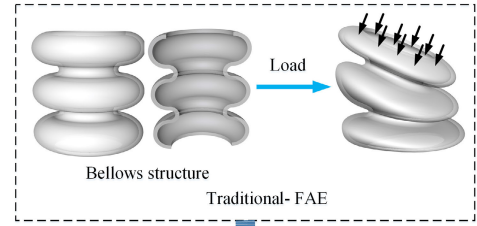


FIGURE 3. Single FAE.

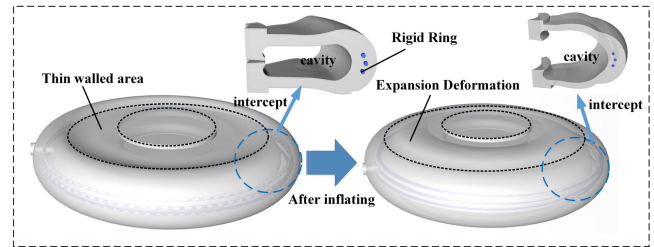


FIGURE 4. Internal structure of single-layer FAU.

When subjected to external pressure load, the load can be adjusted and transferred layer by layer along a certain bending axis to realize the large load and guarantee the driving flexibility and environmental adaptability for the robot.

**C. STRUCTURE OF SINGLE FAU**

Each group of FAE is composed of multi-layer FAUs in parallel, and the internal air pressure of each layer of FAU is independently controlled. The structure of single-layer FAU is shown in Fig. 4, in which the thin-walled area at the upper and lower ends is the expansion and deformation area. When the air pressure is filled into the FAU, the deformation area expands and the FAU extends in the longitudinal direction. The thickness of the radial side edge of the FAU is large, and the rigid spring coil is embedded inside, which can effectively prevent the radial expansion of the FAU during the shape-change expansion, and the driving deformation characteristics of the whole soft robot can be guaranteed.

**III. KINEMATIC MODELING OF PARALLEL SOFT ROBOT**

When no external load is applied to the parallel soft robot and air pressure is applied to the FAU, the thin-walled area will stretch and drive the whole flexible elements to stretch. Fill three groups of FAEs with different air pressure values, the FAEs will stretch different values, the parallel soft robot will realize omnidirectional bending movement as shown in Fig. 5, and define the bending angle of the parallel soft robot as  $\alpha$ , and the deflection angle of moving platform is  $\theta$ .

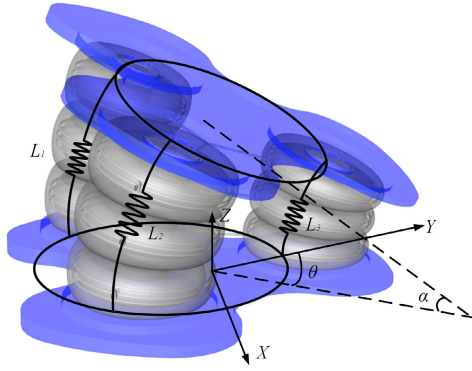


FIGURE 5. Motion attitude of parallel soft robot.

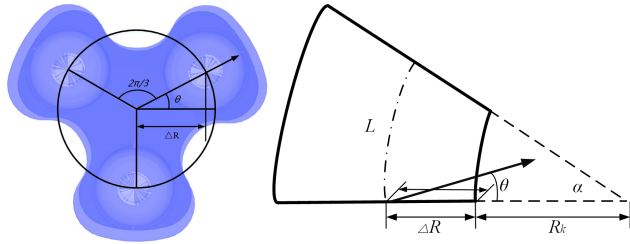


FIGURE 6. The relationship between the distribution of FAE and the length.

The parallel soft robot realizes the elongation or bending movement by changing the length of three groups of FAEs, which are defined as  $L_1$ ,  $L_2$  and  $L_3$ . The centers of the two ends of the three groups of FAEs are evenly distributed in the circle with radius  $R$ , and the three groups of FAEs are evenly distributed at  $120^\circ$ .

When the FAEs are charged with different air pressure values, the parallel soft robot will have bending motion. Firstly, a group of FAE is analyzed. As shown on the left of Fig. 6, the distance between the projection of the center end of the FAE on the fixed platform and the center of the fixed platform circle is  $\Delta R$ . According to the geometric relationship,  $\Delta R$  can be expressed as  $\Delta R = R \cos \theta$ . The center angle of the arc segment of length  $L$  is  $\alpha$ , and  $\Delta R + R_k$  is the radius of the arc. Therefore,  $L/\alpha = \Delta R + R_k$  can be obtained. According to the relationship shown on the right of Fig. 6, we can get  $L_3 = R_k \alpha$ . In summary, we can get:

$$L_3 = \left( \frac{L}{\alpha} - R \cos \theta \right) \alpha = L - R \alpha \cos \theta \quad (1)$$

Similarly,  $L_2$  and  $L_1$  correspond to  $\Delta R_2 = R \cos(\theta + 2\pi/3)$  and  $\Delta R_1 = R \cos(\theta + 4\pi/3)$ . The expressions of  $L_2$  and  $L_1$  are:

$$L_2 = L - R \alpha \cos \left( \frac{2}{3} \pi + \theta \right) = L + R \alpha \left( \frac{1}{2} \cos \theta + \frac{\sqrt{3}}{2} \sin \theta \right) \quad (2)$$

$$L_1 = L - R \alpha \cos \left( \frac{4}{3} \pi + \theta \right) = L + R \alpha \left( \frac{1}{2} \cos \theta - \frac{\sqrt{3}}{2} \sin \theta \right) \quad (3)$$

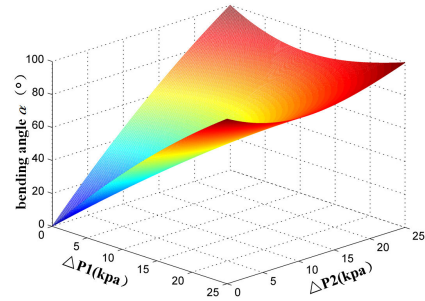


FIGURE 7. mapping relationship between bending angle  $\alpha$  and air pressure.

Three attitude parameters  $\theta$ ,  $\alpha$ ,  $L$  of parallel soft robot are expressed by the length  $L_1$ ,  $L_2$ ,  $L_3$  of three groups of flexible elements, and the relationship between them is obtained.

$$\begin{cases} \theta = a \tan 2 \left( \sqrt{3} L_2 - \sqrt{3} L_3, L_2 + L_3 - L_1 \right) \\ \alpha = \frac{\sqrt{2} [(L_1 - L_2)^2 + (L_2 - L_3)^2 + (L_3 - L_1)^2]}{3R} \\ L = \frac{L_1 + L_2 + L_3}{3} \end{cases} \quad (4)$$

When air pressure is filled into the FAU, the FAU will extend axially. Now, assuming that the air pressure value in the same group of FAU is the same as  $p_i$ , the linear relationship between the FAU and air pressure is obtained as  $\Delta L_i = -0.0161 P_i^2 + 2.1458 P_i + 1.1636$  ( $i = 1, 2, 3$ ) through experimental test. Therefore, the above formula can be rewritten as:

$$\begin{cases} \theta = a \tan 2 \left( \sqrt{3} (\Delta L_2 - \Delta L_3), \Delta L_2 + \Delta L_3 - \Delta L_1 \right) \\ \alpha = \frac{\sqrt{2} [(\Delta L_1 - \Delta L_2)^2 + (\Delta L_2 - \Delta L_3)^2 + (\Delta L_3 - \Delta L_1)^2]}{3R} \\ L = \frac{\Delta L_1 + \Delta L_2 + \Delta L_3}{3} \end{cases} \quad (5)$$

It can be seen from the above formula that there is a mapping relationship between the motion attitude of the parallel robot and the output air pressure, and the control of the motion attitude of the parallel robot can be realized by controlling the input air pressure. When two groups of FAEs are continuously charged with different air pressure, we can get the relationship between the bending angle of parallel soft robot and the input air pressure, as shown in Fig. 7.

#### IV. FORCE ANALYSIS OF PARALLEL SOFT ROBOT

##### A. FORCE ANALYSIS OF FAE

When different air pressure values are input to the FAEs, the state parameters  $\alpha$  and  $\theta$  of the parallel soft robot can be determined in combination with the contents of the previous section. At this time, the external load is applied to the parallel soft robot, and a group of FAE of the parallel soft robot is statically analyzed and modeled. According to the simplified

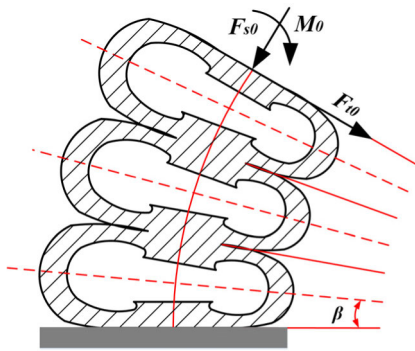


FIGURE 8. Force of FAE in bending state.

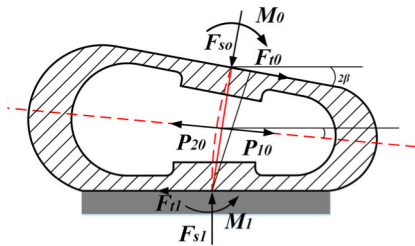


FIGURE 9. Force of FAE in bending state.

force analysis model as shown in Fig. 8, one end of the FAE is fixed and the other end is stressed. In this state, the force analysis is carried out. The single group of FAE is divided into several force analysis units by cross-section method. As shown in Fig. 9, the bending angle of the actuated unit is  $2\beta$ ,  $x$  is the arc length of the central line of the actuated unit, and  $x_0$  is the length of the corresponding secant. The relationship is shown in Formula (6).

$$x_0 = x \sin \beta_0 / \beta_0 \quad (6)$$

Through force analysis,  $F_{s0}$ ,  $M_0$  and  $F_{t0}$  is equivalent to the external force loaded on the moving platform to the fixed surface of the FAU.  $F_{t1}$ ,  $F_{s1}$  and  $M_1$  is the reaction force and moment produced by the next FAU.  $F_{p10}$  and  $F_{p20}$  is the resultant force of the air pressure in the direction away from the bending direction and the bending direction, respectively.

According to the principle of static equilibrium, we can know that the resultant force in the direction of  $F_{s1}$  and  $F_{t1}$  as shown in Fig. 9 is zero, and then the equilibrium equation of force and moment is established.

$$F_{t1} = -F_{s0} \sin 2\beta_0 + (F_{p10} - F_{p20}) \cos \beta_0 + F_{t0} \cos 2\beta_0 \quad (7)$$

$$F_{s1} = F_{s0} \cos 2\beta_0 + (F_{p10} - F_{p20}) \sin \beta_0 + F_{t0} \sin 2\beta_0 \quad (8)$$

$$M_1 = -F_{s0}x_0 \sin \beta_0 + F_{t0}x_0 \cos \beta_0 + (F_{p10} - F_{p20}) \frac{x_0}{2} + M_0 \quad (9)$$

The diameter of the FAE is  $D$ , and the air pressure inside the cavity is  $P$ . Because the pressure generated by the air pressure is always perpendicular to the inner wall of the

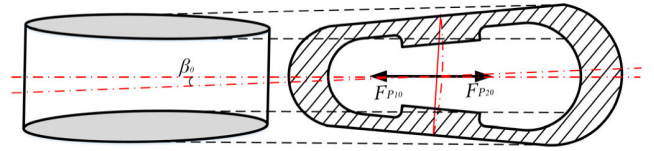


FIGURE 10. Barometric action area.

actuated unit, the bending deformation of the unit under the action of bending moment makes the area difference between the inner and outer surfaces of the bending surface different. As shown in Fig. 10, the area difference will be  $\pi D^2 \sin \beta_0 / 2$ , so formula (10) can be obtained.

$$F_{P1} = (F_{P10} - F_{P20}) = -\frac{P}{2} \pi D^2 \sin \beta_0 \quad (10)$$

The analysis shows that the pressure  $F_{s0}$  includes two parts, one is the force  $F$  of compressed air on the FAU, the other is the actual external load pressure  $F_{load0}$ . The relationship between  $F_{s0}$  and  $F$ ,  $F_{load0}$  is as follows:

$$F_{s0} = F_{load0} - F = F_{load0} - \frac{P}{4} \pi D^2 \quad (11)$$

Formulas (12), (13) and (14) can be obtained by substituting formulas (11) into (7), (8) and (9).

$$F_{t1} = -F_{load0} \sin 2\beta_0 + F_{t0} \cos 2\beta_0 \quad (12)$$

$$F_{s1} = F_{load0} \cos 2\beta_0 - \frac{P}{4} \pi D^2 + F_{t0} \sin 2\beta_0 \quad (13)$$

$$M_1 = -F_{load0}x_0 \sin \beta_0 + F_{t0}x_0 \cos \beta_0 + M_0 \quad (14)$$

By observing equations (12) and (13), it can be found that the magnitude of tangential force  $F_{t1}$  transferred to the next stage is exactly the sum of the component forces of external load pressure  $F_{load0}$  and tangential force  $F_{t0}$  in the direction of  $F_{t1}$ . The pressure  $F_{s1}$  transferred to the next stage is exactly the sum of the component forces of the external load pressure  $F_{load0}$  and tangential force  $F_{t0}$  in the direction of  $F_{s1}$ , and plus the applied force  $F$ . Therefore, we can write equation (13) as:

$$F_{s1} = F_{load1} - \frac{P}{4} \pi D^2 \quad (15)$$

Among them:  $F_{load1} = F_{load0} \cos 2\beta_0 + F_{t0} \sin 2\beta_0$ , which is defined as the external load pressure passed to the next stage. Since the form of Formula (15) is the same as Formula (11),  $F_{load1}$  can be substituted into the equilibrium equation as the next  $F_{load0}$ . Therefore, when the actuated unit has  $n$  layers, it can be concluded that:

$$\begin{cases} F_{tn} = -F_{load(n-1)} \sin 2\beta_{n-1} + F_{t(n-1)} \cos 2\beta_{n-1} \\ F_{sn} = F_{load(n-1)} \cos 2\beta_{n-1} + F_{t(n-1)} \sin 2\beta_{n-1} \\ M_n = -F_{load(n-1)}x_{n-1} \sin \beta_{n-1} \\ \quad + F_{t(n-1)}x_{(n-1)} \cos \beta_{(n-1)} + M_{n-1} \end{cases} \quad (16)$$

Write it in the form of a matrix:

$$\begin{bmatrix} F_{tn} \\ F_{sn} \\ M_n \end{bmatrix} = \begin{bmatrix} \cos 2\beta_{n-1} & -\sin 2\beta_{n-1} & 0 \\ \sin 2\beta_{n-1} & \cos 2\beta_{n-1} & 0 \\ x_{n-1} \cos \beta_{n-1} & -x_{n-1} \sin \beta_{n-1} & 1 \end{bmatrix} \begin{bmatrix} F_{t(n-1)} \\ F_{load(n-1)} \\ M_{n-1} \end{bmatrix} \quad (17)$$

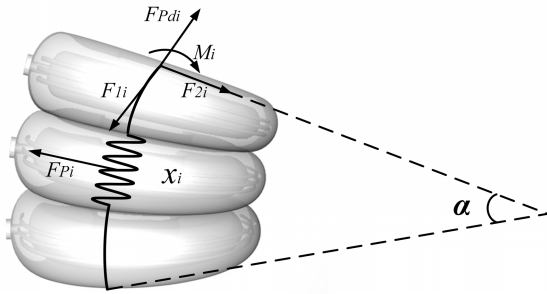


FIGURE 11. Spring model of flexible elements.

If the input force of stage  $n$  is  $(F_{t(n-1)}, F_{load(n-1)}, M_{n-1})$ , then the force transfer matrix of stage  $n$  is  $A_{n-1}$ , then the input force of stage  $m$  can be written as follows:

$$\begin{bmatrix} F_{tm} \\ F_{sm} \\ M_m \end{bmatrix} = A_{m-1}A_{m-2}\dots A_1A_0 \begin{bmatrix} F_{t0} \\ F_{s0} \\ M_0 \end{bmatrix} = \prod_{n=1}^m A_{n-1} \begin{bmatrix} F_{t0} \\ F_{s0} \\ M_0 \end{bmatrix} \quad (18)$$

The expression of  $\prod_{n=1}^m A_{n-1}$  in formula (18) is:

$$\prod_{n=1}^m A_{n-1} = \begin{bmatrix} \cos \sum_{n=1}^m 2\beta_n & -\sin \sum_{n=1}^m 2\beta_n & 0 \\ \sin \sum_{n=1}^m 2\beta_n & \cos \sum_{n=1}^m 2\beta_n & 0 \\ B_m & C_m & 1 \end{bmatrix} \quad (19)$$

From the formula analysis, it can be seen that the positive pressure transmitted on each connection surface is related to the external load and the tangential force. The larger the external load, the greater the positive pressure transmitted and the greater the tangential force transmitted.

### B. FORCE ANALYSIS AND MODELING OF PARALLEL ROBOT

The flexible element is regarded as a special flexible spring which can be stretched, bended and the bending curve is an arc with equal curvature as shown in Fig. 11. Fixed one end of the  $i$ -th flexible element and applied pressure  $F_{si}$ , tangential force  $F_{ti}$  and moment  $M_{bi}$  at the other end. The inner wall of the flexible element is subjected to gas pressure. The effect can be regarded as pressure  $F_{pdi} = \pi PD^2/4$  along the tangent at the active end of the spring and pressure  $F_{pi} = \frac{P}{2}\pi D^2 \sin\alpha/2$  at the middle point of the spring and outward along the normal of the point. Because of the existence of pressure, if the length is  $x_i$  and the bending angle is  $\alpha_i$ , the applied external force should be as follows:

$$\begin{cases} F_{1i} = F_{pdi} - \sin(0.5\alpha) F_{pi} = \frac{1}{4}\Delta P_i \pi D^2 \\ \quad - \frac{1}{2}\pi \Delta P_i D^2 \sin(0.5\alpha)^2 \\ F_{2i} = \cos(0.5\alpha) F_{pi} = \frac{1}{2}\pi \Delta P_i D^2 \cos(0.5\alpha) \sin(0.5\alpha) \\ M_i = -F_{pi} \frac{L_i}{\alpha} \sin(0.5\alpha) = -\frac{1}{2}\pi \Delta P_i D^2 \frac{x_i}{\alpha} \sin^2(0.5\alpha) \end{cases} \quad (20)$$

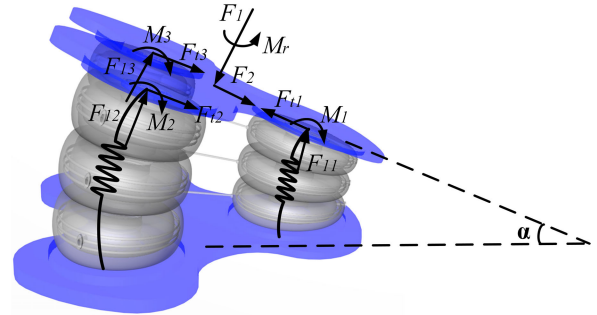


FIGURE 12. A simplified model of bending force.

Because the torsion of the flexible elements is similar to the rigidity, the parallel soft robot composed of the flexible elements is also rigid to the torsion, that is to say, there is no torsion deformation but only elongation and bending deformation. It is assumed that the pressure on the moving platform of the robot is  $F_1$  perpendicular to the upper end surface and outward through the center of the upper end surface,  $F_2$  is the tangential force pointing to the center of the bending circle at the intersection of the bending plane and the upper end surface,  $M$  is the bending moment perpendicular to the upper end surface, and  $M_r$  is the torque that is outward through the center of the upper end surface. Under the action of these forces, the three FAEs of the parallel soft robot bend angle  $\alpha$ , and their lengths change to  $x_1, x_2$  and  $x_3$  respectively. The three FAEs have the same internal pressure of  $P_{1i}, P_{2i}$  and  $P_{3i}$  respectively. The combined spring model of the external force and the FAE of the mobile platform of the robot is shown in the Fig. 12.

The three pressures  $F_{1i}$  are perpendicular to the upper end surface, and the three directions of pressures are defined as opposite to  $F_1$ . The force balance equation of the sum of three pressures and the external load pressure can be obtained.

$$F_{11} + F_{12} + F_{13} = F_1 \quad (21)$$

Three pressures generate moments about axes passing through the center of the moving platform and perpendicular to the bending plane. And the equilibrium equation of the sum of the moment produced by the moment and the external load and the moment exerted by the flexible elements on the moving platform:

$$F_{11}R \cos\theta + F_{12}R \cos\left(\theta + \frac{2}{3}\pi\right) + F_{13}R \cos\left(\theta + \frac{4}{3}\pi\right) = M - M_1 - M_2 - M_3 \quad (22)$$

The overturning moment of three pressures deviating from the bending plane exists at the intersection of the moving platform and the bending plane. The sum of these moments is zero, and the equilibrium equation is given as follows:

$$F_{11}R \sin\theta + F_{12}R \sin\left(\theta + \frac{2}{3}\pi\right) + F_{13}R \sin\left(\theta + \frac{4}{3}\pi\right) = 0 \quad (23)$$

Write these three equations in matrix form (24), as shown at the bottom of the next page.

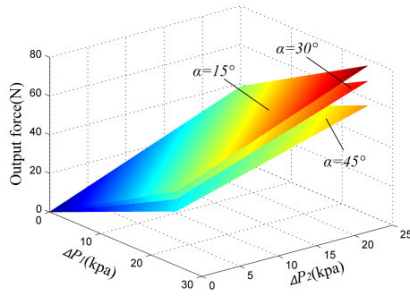


FIGURE 13. The relationship between  $\Delta P_1$ ,  $\Delta P_2$  and  $F$  at different bending angles.

The solution is obtained.

$$\begin{cases} F_{11} = \frac{F_1}{3} + \frac{2 \left( M - \sum_{i=1}^3 M_i \right) \cos \theta}{3r} \\ F_{12} = \frac{F_1}{3} + \frac{2 \left( M - \sum_{i=1}^3 M_i \right) \left( -0.5\sqrt{3} \sin \theta - 0.5 \cos \theta \right)}{3r} \\ F_{13} = \frac{F_1}{3} + \frac{2 \left( M - \sum_{i=1}^3 M_i \right) \left( 0.5\sqrt{3} \sin \theta - 0.5 \cos \theta \right)}{3r} \end{cases} \quad (25)$$

When the FAE is filled with a certain amount of air pressure, the parallel flexible robot is fixed in the bending state. Through the above analysis, we can derive equation 26, from which we can get the relationship between the output force, the output bending moment and the pressure increment under the condition of fixed bending deformation.

$$\begin{cases} \Delta P_1 = \frac{F_1/3 + 2 \left( M - \sum_{i=1}^3 M_i \right) \cos \theta / 3r}{\pi D^2/4 - \pi D^2 \sin(0.5\alpha)^2/2} \\ \Delta P_2 = \frac{F_1/3 + 2 \left( M - \sum_{i=1}^3 M_i \right) \left( -0.5\sqrt{3} \sin \theta - 0.5 \cos \theta \right) / 3r}{\pi D^2/4 - \pi D^2 \sin(0.5\alpha)^2/2} \\ \Delta P_3 = \frac{F_1/3 + 2 \left( M - \sum_{i=1}^3 M_i \right) \left( 0.5\sqrt{3} \sin \theta - 0.5 \cos \theta \right) / 3r}{\pi D^2/4 - \pi D^2 \sin(0.5\alpha)^2/2} \end{cases} \quad (26)$$

After the bending motion of the parallel soft robot is deformed to a certain posture, the first and second groups of FAEs are selected to be filled with air pressure. When the bending angle  $\alpha$  is 15, 30 and 45 degrees, the relationship between the output force and the pressure increment of the two groups of FAE is shown in Fig. 13. It can be concluded from the figure that the larger  $\alpha$  is, the smaller the output force is.

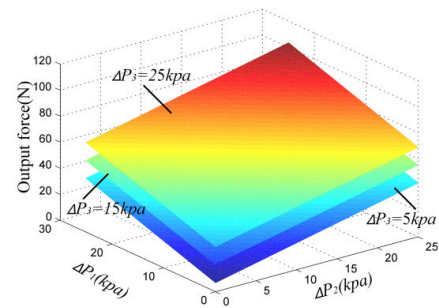


FIGURE 14. The relationship between  $\Delta P_1$ ,  $\Delta P_2$  and  $F$  under different  $\Delta P_3$ .

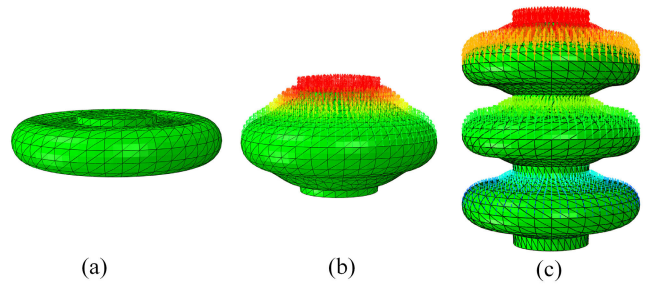


FIGURE 15. (a) Before deformation of FAU. (b) After deformation of FAU. (c) Deformation of FAE.

The relationship between the output force and the pressure increment of the other two groups of flexible components is shown in Fig. 14, when the bending angle is 30 degrees and the pressure increment of the third group is 5 kPa, 15 kPa and 25 kPa, respectively. It can be seen from the figure that when the bending angle  $\alpha$  of the moving platform is the same, the greater the sum of the pressure increments of the FAE, the greater the output force.

## V. FINITE ELEMENT SIMULATION VERIFICATION

In this paper, rubber with the characteristics of large non-linear deformation is chosen as the flexible material. Firstly, the silicone rubber material is defined as a hyperelastic body, and the second-order Yeoh model [29] is adopted. Then, one end of the actuated unit is fixed. Finally, the parallel soft robot is simulated by adding air pressure load.

The actuated element is modeled then and imported into Abaqus software to adjust the actuated unit and actuated element model uniformly to add pressure to the surface of the cavity. When the pressure is gradually applied to the surface of the cavity to 45 kPa, its deformation is shown in Fig. 15. It can be seen from the figure that the deformation is basically consistent with the anticipated structural design, and the radial deformation is small, but the deformation effect in the thin-walled deformation area is obvious.

$$\begin{bmatrix} 1 & 1 & 1 \\ R \cos \theta - 0.5R \left( \cos \theta + \sqrt{3} \sin \theta \right) & -0.5R \left( \cos \theta - \sqrt{3} \sin \theta \right) & \\ R \sin \theta - 0.5R \left( \sin \theta - \sqrt{3} \cos \theta \right) & -0.5R \left( \sin \theta + \sqrt{3} \cos \theta \right) & \end{bmatrix} \begin{bmatrix} F_{11} \\ F_{12} \\ F_{13} \end{bmatrix} = \begin{bmatrix} F_1 \\ M - \sum_{i=1}^3 M_i \\ 0 \end{bmatrix} \quad (24)$$

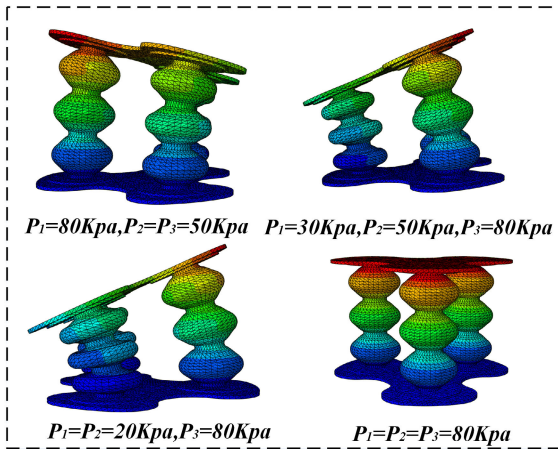


FIGURE 16. Simulate the bending deformation of soft robot.

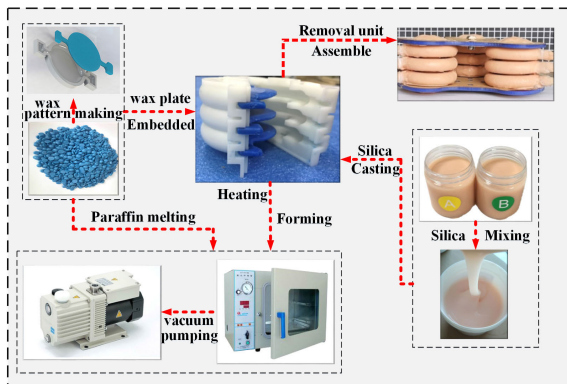


FIGURE 17. Prototype manufacturing process.

In the same way, the multi-DOF parallel soft robot is simulated and analyzed. One of the platforms is set as a fixed platform, and three groups of flexible-actuated components are fed into different air pressure values. The simulation results are shown in Fig. 16. It can be seen from the graph that when the air pressure inside the FAU is changed, the moving platform of the parallel soft robot will have deflection displacement at different angles.

## VI. EXPERIMENT

### A. DEVELOPMENT OF EXPERIMENTAL PROTOTYPE

An experimental prototype of Multi-DOF Parallel Soft Robot was made. Firstly, the mould was made by 3D printing technology and the wax model was made by casting wax. Then the wax mold is embedded in the printed silica gel mold, and the uniformly mixed silica gel is poured into the combined silica gel mold. After the silica gel model is formed, it is removed and the internal wax plates are melted. Finally, a FAE is formed and assembled into a parallel soft robot. The manufacturing process is shown in Fig. 17.

### B. MOTION DEFORMATION EXPERIMENTS OF PROTOTYPE

Motion detection and control system is built. Pneumatic proportional valve is used to continuously control the output air

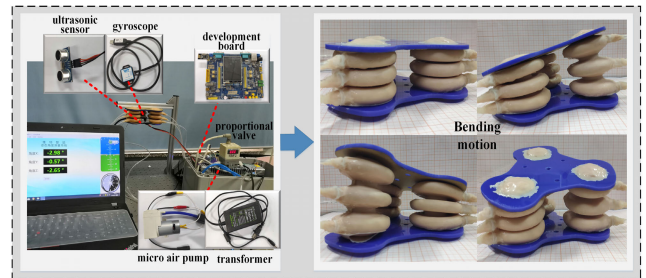


FIGURE 18. Measurement of omnidirectional bending movement.

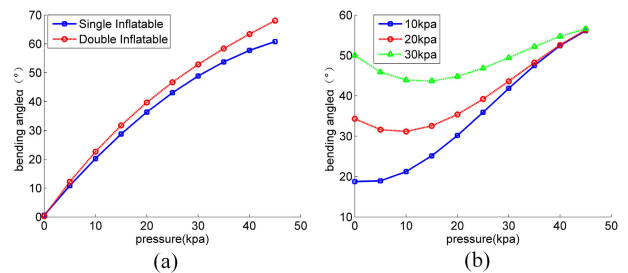


FIGURE 19. (a) Single/double group inflation pressure and bending angle, (b) Pressure and bending angle of two groups of unequal pressure.

pressure of the pump, and the proportional valve is controlled by single-step by single chip computer. The ultrasonic distance sensor and gyroscope are mounted on the moving end of the parallel soft robot. Different air pressure is applied to the three groups of FAEs. The parallel soft robot will bend at different angles as shown in Fig. 18.

Firstly, select one or two groups of flexible elements in the prototype and charge them with air pressure to form bending movement. Measure the bending deflection angle of the prototype under different pressure by gyroscope. The experimental results are shown in Fig. 19(a). Select two groups of flexible elements in the prototype randomly and fill them with air pressure. Keep the pressure in the cavity of one group of flexible elements as 10kpa, 20 kpa and 30 kpa respectively. Measure the bending deflection angle of the prototype of the other group of flexible elements under different pressures. The experimental results are shown in Fig. 19(b).

The experiment of prototype deformation motion verifies that the robot can realize all-direction bending motion which is concluded that the bending angle of the prototype can reach 60 degrees when inflating to a single group of FAE, and 67 degrees when inflating to two groups of FAEs. The bending angle of the moving platform is slightly larger when the same pressure is applied to the two groups of FAEs than to the single group of FAE. This is because when inflated to the FAE, the other FAE that is not inflated will also bend and deform. When inflating a single group of FAE, two other groups of non-inflatable FAEs hinder their deformation. When inflating two groups of FAEs, the single group of non-inflatable FAE hinders their movement and deformation.

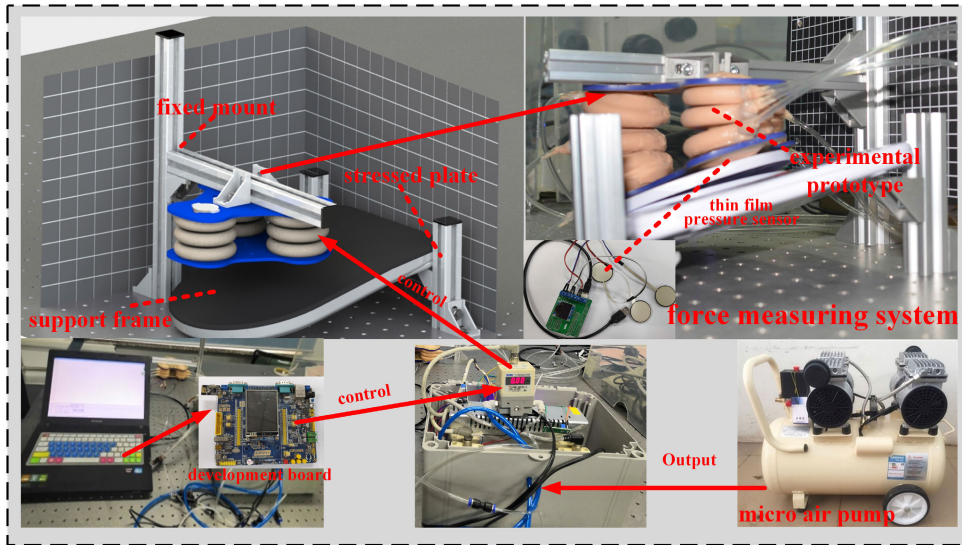


FIGURE 20. Output force measurement.

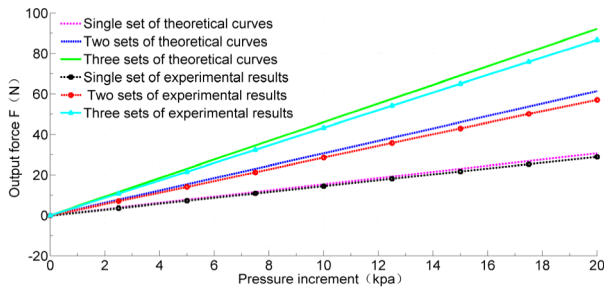


FIGURE 21. Single group bending 15 degrees.

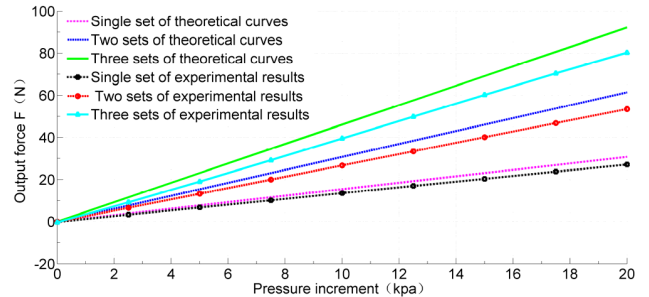


FIGURE 23. Double bending 15 degrees.

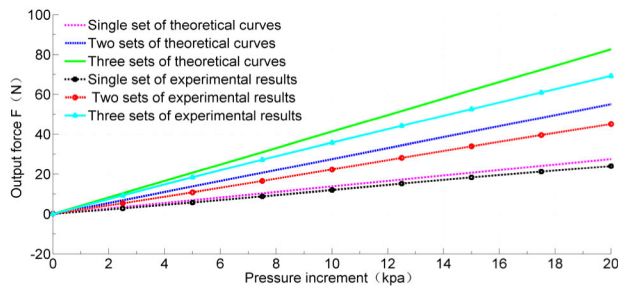


FIGURE 22. Single group bending 30 degrees.

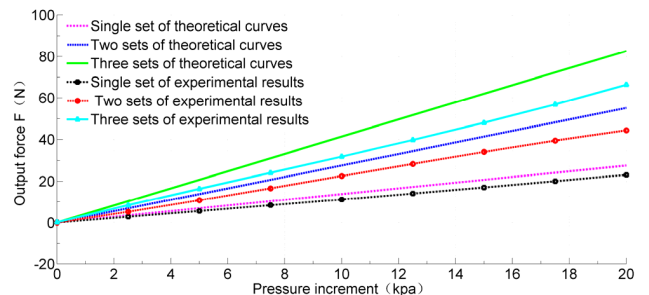


FIGURE 24. Double bending 30 degrees.

**C. OUTPUT FORCE MEASUREMENT OF PROTOTYPE**

A force measurement experiment platform is built as shown in Fig. 20. Three thin film pressure sensors are attached to the corresponding force output positions of the FAEs of the robot, and the data are recorded in real time by computer. The support frame is used to place the stressed plate with different inclination angles, and the fixing mount is used to fix the fixed platform of the experimental prototype. And through the air pressure control system, the air pressure inside the FAE can be controlled in real time. When a group of FAE is inflated with air pressure to make the bending of the robot reach 15 degrees and 30 degrees respectively, the support frame is adjusted to make the stressed plate and the moving platform fit together so that the robot's attitude is fixed.

In these two fixed states, the incremental bearing capacity at different pressures is obtained by pressurizing one group, two groups and three groups of FAEs. Finally, the experimental results of inflating in one, two and three groups of FAEs are obtained and compared with the theoretical values, as shown in Fig. 21 and Fig. 22.

When inflated with two groups of flexible elements, the initial bending deflection angles  $\alpha$  of the platform are 15 and 30, and the experimental results are compared with the theoretical values under the two fixed states, as shown in Fig. 23 and Fig. 24.

Experiments show that the designed flexible parallel soft robot with large load also has large load-carrying capacity in bending state. The results show that the output force increases

linearly with the increase of pressure increment, and the maximum output force can be obtained when the three groups of flexible components are pressurized at the same time.

## VII. CONCLUSION

In this paper, a novel type of multi-DOF parallel soft robot, made of soft material and pneumatic-driven, is proposed with the advantages of light weight, strong environmental adaptability and high safety coefficient. With parallel mechanism, flexible drive with large load is realized by the increase of connection area between FAUs. Kinematic and force coupled analysis was carried out and the mapping model of kinematic attitude parameters and the external load force with output air pressure value is established to realize facilitated control over the motion and output force of the robot. In addition, the combination of finite element analysis and prototype experiment is carried out to verify the ability of multi-DOF omnidirectional bending motion and flexible drive with large load of the soft robot. In the future applications, the robot can be used as a soft grabbing robot to grab objects of different shapes and sizes. It can be combined with a rigid robot to directly contact with the human body as the executive end. At the same time, it can also rely on its flexible deformation ability to combine with the search and rescue machine and human to perform the exploration task of complex landform.

## REFERENCES

- [1] D. Trivedi, C. D. Rahn, W. M. Kier, and I. D. Walker, "Soft robotics: Biological inspiration, state of the art, and future research," *Appl. Bionics Biomech.*, vol. 5, no. 3, pp. 99–117, Dec. 2008, doi: [10.1080/11762320802557865](https://doi.org/10.1080/11762320802557865).
- [2] F. Iida and C. Laschi, "Soft robotics: Challenges and perspectives," *Procedia Comput. Sci.*, vol. 7, pp. 99–102, May 2011, doi: [10.1016/j.procs.2011.12.030](https://doi.org/10.1016/j.procs.2011.12.030).
- [3] G. Chen, M. T. Pham, and T. Redarce, "Sensor-based guidance control of a continuum robot for a semi-autonomous colonoscopy," *Robot. Auton. Syst.*, vol. 57, nos. 6–7, pp. 712–722, Jun. 2009, doi: [10.1016/j.robot.2008.11.001](https://doi.org/10.1016/j.robot.2008.11.001).
- [4] I. D. Walker, "Continuous backbone 'continuum' robot manipulators," *Isrn Robot.*, vol. 2013, Jun. 2013, Art. no. 726506.
- [5] S. Neppalli, B. Jones, W. McMahan, V. Chitrakaran, I. Walker, M. Pritts, M. Csencsits, C. Rahn, and M. Grissom, "OctArm—A soft robotic manipulator," in *Proc. IEEE/RISJ Conf. Intell. Robots Syst.*, San Diego, CA, USA, Oct./Nov. 2007, p. 2569.
- [6] J. S. Mehlring, M. A. Diftler, M. Chu, and M. Valvo, "A minimally invasive tendril robot for in-space inspection," in *Proc. IEEE/RAS-EMBS Int. Conf. Biomed. Robot. Biomechtron.*, Pisa, Italy, Feb. 2006, pp. 690–695, doi: [10.1109/BIOROB.2006.1639170](https://doi.org/10.1109/BIOROB.2006.1639170).
- [7] C. Cheng, J. Cheng, and W. Huang, "Design and development of a novel SMA actuated multi-DOF soft robot," *IEEE Access*, vol. 7, pp. 75073–75080, 2019, doi: [10.1109/ACCESS.2019.2920632](https://doi.org/10.1109/ACCESS.2019.2920632).
- [8] W.-B. Li, W.-M. Zhang, and X.-Q. Li, "Design and experiment of an omnidirectional creeping soft robot driven by dielectric elastomer," *Proc. SPIE*, vol. 10594, Mar. 2018, Art. no. 105941R, doi: [10.1117/12.2296553](https://doi.org/10.1117/12.2296553).
- [9] R. Mutlu, G. Alici, and W. Li, "Electroactive polymers as soft robotic actuators: Electromechanical modeling and identification," in *Proc. IEEE/ASME Int. Conf. Adv. Intell. Mechatronics*, Wollongong, NSW, Australia, Jul. 2013, pp. 1096–1101, doi: [10.1109/AIM.2013.6584240](https://doi.org/10.1109/AIM.2013.6584240).
- [10] J. Zhang, H. Guo, T. Wang, and J. Hong, "The design and motion analysis of a pneumatic omnidirectional soft robot," *Int. J. Robot. Automat.*, vol. 32, no. 6, pp. 569–576, 2017, doi: [10.2316/Journal.206.2017.6.206-4908](https://doi.org/10.2316/Journal.206.2017.6.206-4908).
- [11] J. A. Rivera and C. J. Kim, "Spatial parallel soft robotic architectures," in *Proc. IEEE/RISJ Int. Conf. Intell. Robots Syst.*, Sep. 2014, pp. 548–553, doi: [10.1109/IROS.2014.6942613](https://doi.org/10.1109/IROS.2014.6942613).
- [12] J. B. Hopkins, J. Rivera, C. Kim, and G. Krishnan, "Synthesis and analysis of soft parallel robots comprised of active constraints," *J. Mech. Robot.*, vol. 7, no. 1, Feb. 2015, Art. no. 011002, doi: [10.1115/1.4029324](https://doi.org/10.1115/1.4029324).
- [13] J. Rivera, J. B. Hopkins, and C. Kim, "Synthesizing soft parallel robots comprised of active constraints," in *Proc. Int. Design Eng. Tech. Conf. Comput. Inf. Eng. Conf.*, Aug. 2014, pp. 1–11, doi: [10.1115/DETC2014-34551](https://doi.org/10.1115/DETC2014-34551).
- [14] D. Drotman, M. Ishida, S. Jadhav, and M. T. Tolley, "Application-driven design of soft, 3-D printed, pneumatic actuators with bellows," *IEEE/ASME Trans. Mechatronics*, vol. 24, no. 1, pp. 78–87, Feb. 2019, doi: [10.1109/TMECH.2018.2879299](https://doi.org/10.1109/TMECH.2018.2879299).
- [15] R. J. Webster and B. A. Jones, "Design and kinematic modeling of constant curvature continuum robots: A review," *Int. J. Robot. Res.*, vol. 29, no. 13, pp. 1661–1683, Nov. 2010, doi: [10.1177/0278364910368147](https://doi.org/10.1177/0278364910368147).
- [16] V. Falkenhahn, T. Mahl, A. Hildebrandt, R. Neumann, and O. Sawodny, "Dynamic modeling of constant curvature continuum robots using the Euler-Lagrange formalism," in *Proc. IEEE/RISJ Int. Conf. Intell. Robots Syst.*, Oct. 2014, pp. 2428–2433, doi: [10.1109/IROS.2014.6942892](https://doi.org/10.1109/IROS.2014.6942892).
- [17] R. K. Katzschmann, C. D. Santana, Y. Tshimitsu, A. Bicchi, and D. Rus, "Dynamic motion control of multi-segment soft robots using piecewise constant curvature matched with an augmented rigid body model," in *Proc. 2nd IEEE Int. Conf. Soft Robot. (RoboSoft)*, Apr. 2019, pp. 454–461, doi: [10.1109/ROBOSOFT.2019.8722799](https://doi.org/10.1109/ROBOSOFT.2019.8722799).
- [18] M. Dehghani and S. A. A. Moosavian, "Static modeling of continuum robots by circular elements," in *Proc. 21st Iranian Conf. Electr. Eng. (ICEE)*, Mashhad, Iran, May 2013, pp. 1–6, doi: [10.1109/IranianCEE.2013.6599741](https://doi.org/10.1109/IranianCEE.2013.6599741).
- [19] M. Dehghani and S. A. A. Moosavian, "Modeling of continuum robots with twisted tendon actuation systems," in *Proc. 1st RSJ/ISM Int. Conf. Robot. Mechatronics (ICRoM)*, Feb. 2013, pp. 14–19, doi: [10.1109/ICRoM.2013.6510074](https://doi.org/10.1109/ICRoM.2013.6510074).
- [20] Z. Gong, Z. Xie, X. Yang, T. Wang, and L. Wen, "Design, fabrication and kinematic modeling of a 3D-motion soft robotic arm," in *Proc. IEEE Int. Conf. Robot. Biomimetics (ROBIO)*, Qingdao, China, Dec. 2016, pp. 509–514.
- [21] X. Wang, T. Geng, Y. Elsayed, C. Saaj, and C. Lekakou, "A unified system identification approach for a class of pneumatically-driven soft actuators," *Robot. Auton. Syst.*, vol. 63, pp. 136–149, Jan. 2015.
- [22] P. Qi, C. Qiu, H. Liu, J. S. Dai, L. D. Seneviratne, and K. Althoefer, "A novel continuum manipulator design using serially connected double-layer planar springs," *IEEE/ASME Trans. Mechatronics*, vol. 21, no. 3, pp. 1281–1292, Jun. 2016.
- [23] Z. Zhang, X. Wang, S. Wang, D. Meng, and B. Liang, "Design and modeling of a parallel-pipe-crawling pneumatic soft robot," *IEEE Access*, vol. 7, pp. 134301–134317, Sep. 2019.
- [24] D. B. Reynolds, D. W. Repperger, C. A. Phillips, and G. Bandry, "Modelling the dynamic characteristics of pneumatic muscle," *Ann. Biomed. Eng.*, vol. 31, no. 3, pp. 310–317, Mar. 2003.
- [25] R. J. Webster and B. A. Jones, "Design and kinematic modeling of constant curvature continuum robots: A review," *Int. J. Robot. Res.*, vol. 29, no. 13, pp. 1661–1681, Jun. 2010, doi: [10.1177/0278364910368147](https://doi.org/10.1177/0278364910368147).
- [26] B. A. Jones and I. D. Walker, "Kinematics for multisection continuum robots," *IEEE Trans. Robot.*, vol. 22, no. 1, pp. 43–55, Feb. 2006.
- [27] J. Wang, K.-L. Ting, Y. Gong, and H. He, "Motion continuity and branch identification of two-dof seven-bar planar parallel manipulators and linkages," *Int. J. Robot. Automat.*, vol. 34, no. 4, pp. 397–409, 2019.
- [28] W. D. Yu, H. Wang, and G. L. Chen, "Design and kinematic analysis of a 3-translational-DOF spatial parallel mechanism based on polyhedra," *Mech. Mach. Theory*, vol. 121, pp. 92–115, Mar. 2018, doi: [10.1016/j.mechmachtheory.2017.10.020](https://doi.org/10.1016/j.mechmachtheory.2017.10.020).
- [29] A. K. Mohammadi and S. D. Barforooshi, "Nonlinear forced vibration analysis of dielectric-elastomer based micro-beam with considering yeoh hyper-elastic model," *Latin Amer. J. Solids Struct.*, vol. 14, no. 4, pp. 643–656, Mar. 2017, doi: [10.1590/1679-78253324](https://doi.org/10.1590/1679-78253324).



**JIE ZHANG** received the B.S. degree in statistics from the College of Science, Yanshan University, China, in 2003, where she is currently pursuing the Ph.D. degree in control science and engineering. She is also a Lecturer with the Liren College, Yanshan University. Her current research interests include the system identification of fractional order systems and robot control theory.



**HANG WEI** received the B.S. degree in mechanical and electronic engineering from the Liren College, Yanshan University, Qinhuangdao, China, in 2018, where he is currently pursuing the M.S. degree in mechatronics engineering. His current research interests include multi DOF parallel soft robots and variable rigidity soft robots.



**YANZHI ZHAO** received the B.S. degree in mechanical engineering and the Ph.D. degree in mechatronics engineering from Yanshan University, Qinhuangdao, China, in 2003 and 2009, respectively. He is currently a Professor with the Department of Mechatronics Engineering, Yanshan University. His current research interests include parallel multi dimensional force sensors, and theory and applications of parallel manipulators.



**YU SHAN** received the B.S. degree in mechanical and electronic engineering from Yanshan University, Qinhuangdao, China, in 2017, where he is currently pursuing the M.S. degree in mechatronics engineering. His research interests include theory and applications of parallel manipulators and variable rigidity robots.



**LIZHE QI** received the B.S. degree from Yanshan University, Qinhuangdao, China, in 2003, the M.S. degree from the Harbin Institute of Technology, Harbin, China, in 2005, and the Ph.D. degree from Beihang University, Beijing, China, in 2014, all in mechanical engineering. He is currently a Researcher with Fudan University, Shanghai. His research interests are robot vision, robotflexible control, and intelligent industrial robot systems.



**PENGBO LI** received the B.S. degree in mechanical engineering from the Hebei University of Science and Technology, Shijiazhuang, China, in 2016, and the M.S. degree in mechatronics engineering from Yanshan University, Qinhuangdao, China, in 2019. His current research interest includes flexible drive soft massage robots.



**HONGNIAN YU** received the B.S. degree in industrial automation from the Harbin Institute of Technology, Harbin, China, in 1982, the M.S. degree industrial automation from the Northeast Heavy Machinery Institute, Qiqihar, China, 1985, and the Ph.D. degree in mechatronics engineering from the University of London, London, U.K., in 1994. He is currently a Professor with the School of Engineering and Built Environment, Edinburgh Napier University. His current research interest includes intelligent control and robots.

...